Angewandte Chemie
Eine Zeitschrift der Gesellschaft Deutscher Chemiker

Supporting Information

© Wiley-VCH 2014

69451 Weinheim, Germany

Boron Clusters as Highly Stable Magnesium-Battery Electrolytes**

Tyler J. Carter, Rana Mohtadi, Timothy S. Arthur, Fuminori Mizuno, Ruigang Zhang, Soichi Shirai, and Jeff W. Kampf*

ange_201310317_sm_miscellaneous_information.pdf

Contents Page #

Experimental Details

General Methods:

All experiments were conducted in an argon filled glovebox or on a nitrogen Schlenk line. All solvents were purchased in anhydrous form from Sigma Aldrich or Cambridge Isotope Labs (deuterated solvents) and used as received. Magnesium borohydride, decaborane, and isopropyl Grignard solution (2.0 M in Et_2O) were purchased from Sigma Aldrich and *m*-carborane was purchased from Alfa Aesar and used as received.

Infrared Analysis

To prevent exposure to air during the analysis, an air tight Specac Smart Golden Gate ATR™ cell equipped with a diamond crystal was used in all IR analyses which were run using a Nicolet 8700 FT-IR (by Thermo Scientific).

NMR Spectra

NMR analysis was conducted on a Varian MR400 MHz spectrometer. ^{1}H NMR spectra were referenced relative to the protic solvent resonance, and ^{11}B spectra are referenced indirectly based on the ^{1}H spectrum.[1] As previously observed for other boron containing compounds,[2] the boron bound carbons in the carborane scaffold could not be resolved due to quadrapolar coupling, thus ^{13}C NMR spectra are not reported.

Electrochemical Analysis

All electrochemical experiments were conducted using a Bio-Logic VMP3 multi-channel potentiostat. Electrolyte solutions for experiments with **2** were carried out with bulk material at a concentration of 100 mg/ml unless otherwise specified. For cyclic and linear scan voltammetry on mixture **1**, propylene carbonate was used as the solvent (17 mg/ml concentration). A fresh electrolyte solution was prepared for each experiment. Working electrodes were Pt, Al, Ni, and 316-Stainless Steel, and were extensively polished between each use. Unless otherwise stated, counter and reference electrodes were magnesium ribbon and wire. Cyclic voltammetry and linear scan voltammetry experiment were conducted at a scan rate of 5 mV/sec. Oxidation onset potentials and coulombic efficiencies were determined using previously described methods.[3] Chronoamperometry was conducted by holding a Pt working electrode at predetermined voltages and recording the measured current values with time. The 0.4:0.2 M $PhMgCl:AlCl_3$ and Chevrel phase Mo_6S_8 cathode were prepared as was described in literature.[4] Conductivity measurements were conducted using a Pt electrode symmetrical cell. The cell constant was obtained by cell calibration using potassium chloride and was used to calculate to conductivity of the electrolyte.

Galvanostatic Deposition

The galvanostatic deposition of magnesium was conducted using a teflon three electrode cell with a platinum disk working electrode and a magnesium disk counter electrode. A constant current corresponding to a potential of -0.7 V (vs. Mg) was applied for 100 h, before the cell was deconstructed, and platinum disk washed with THF. The disk was then analyzed by X-ray diffraction to verify the deposition of magnesium.

Powder X-ray Diffraction

X-ray diffraction was conducted in Rigaku SmartLab® equipped with Cu Kα X-ray source. Prior to the X-ray analysis, the platinum disk obtained following galvanostatic deposition of magnesium was carefully covered with 8 μm Kapton film to prevent exposure to air. All experiments were run at 0.3° /min scan rate and 0.02° step size. The ex-situ XRD result shown in SI figure 11 was run for the pristine, as prepared, Chevrel phase electrode and following the 1st discharge. The discharged battery was disassembled under Ar in a glove box and the cathode electrode was completely rinsed with THF and dried under vacuum at 25 ^{o}C for 1 hour to remove any residual solvent in the electrode. The discharged electrode was then sealed in an air free sample holder with beryllium window during the XRD analysis.

Battery Testing:

Battery experiments were conducted in Tom-Cells™ using a magnesium disk anode and Chevrel phase cathode with a glassy carbon current collector. The cathode consisted of 70% Mo_6S_8, 20% carbon black and 10% PTFE binder. The electrode was prepared by grinding the mixture using a mortar and pestle with the addition of 5 ml ethanol for 30 minutes. The resulting soft block mixture was pressed into a 120 μm sheet via a press roller and dried overnight at 120 ^{o}C under vacuum. The cathode pellets were cut out from the sheet at 13 mm diameter (1.33 cm^2 area). The cell was assembled in the glove box and run at room temperature. Charge and discharge experiments were conducted at a constant current of ± 25 μA. Each electrode pellet was tested in a customized Tomcell (TJ-AC Tomcell Japan) using a 0.2 μm thick (28 mm diameter) standard glass filter (Sigma-Aldrich) as a separator and a Mg foil (19 mm diameter) as the counter and reference electrodes. Mg foil was polished by scraping each side of the foil with sandpaper and wiping clean with a Kimwipe (Kimberly-Clark). All cells were assembled under Ar in a glovebox (<0.1 ppm of water and oxygen).

DFT Calculations:

The reduction potentials vs SHE ($E°_{red}$) for the reactions $B_nH_n^{0/-/2-} + e- \rightarrow B_nH_n^{-/2-/3-}$ were obtained by using a known computational procedure.[5] All calculations were carried out using the Gaussian09 program.[6] The density functional theory (DFT) method with B3LYP exchange-correlation functional was used for all calculations.[7] The basis set adopted was 6-311++G(d,p).[8] First, the adiabatic electron affinities were calculated from the free energies of electron attachment in the gas phase ($\Delta G_{E.A.}$). The molecular geometries were optimized, and zero-point energies, thermal energies and entropy corrections were performed by using the vibrational calculations (temperature set to 298.15 K). The solvation free energies (ΔG_{solv}) were also calculated at the optimized geometries using the conductor-like polarizable continuum model (CPCM)[9] with the Pauling cavity set.[6] The assumed solvent was water (dielectric constant, ε = 78.35) and terahydrofuran (THF, ε = 7.43). The solvent excluded surface (SES) technique was applied with an average density integration point of 10 $Å^{-2}$. The electron attachment in the solution (ΔG_{sol}) can be calculated using the equation, $\Delta G_{sol} = \Delta G_{E.A.} + \Delta\Delta G_{solv}$, where $\Delta\Delta G_{solv}$ is the change in the solvation free energy. The absolute reduction potential, $E°_{abs}$, was calculated using the equation, $E°_{abs} = -\Delta G_{sol} / nF$, where F is Faraday's constant and n is the number of moles of electrons transferred per mol of reactant. Finally, $E°_{red}$ was obtained using the equation, $E°_{red} = E°_{abs} - 4.28$, where the absolute value of SHE was assumed to be 4.28 V.[5, 10] The calculated $E°_{red}$ values are collected in SI Table 1. The electronic state energies are summarized in SI Table 2. The calculated $\Delta G_{E.A.}$, $\Delta\Delta G_{solv}$, ΔG_{sol} and $E°_{abs}$ values for the reactions in water and tetrahydrofuran are summarized in SI Table 3.

SI Table 1: Calculated reduction potentials ($E°_{red}$, V) vs SHE.[a]

	Water (ε = 78.35)	THF (ε = 7.43)	Gas Phase (ε = 0.0)
$BH_4 + e^- \rightarrow [BH_4]^-$	1.54	1.20	−1.20
$BF_4 + e^- \rightarrow [BF_4]^-$	5.16	4.89	2.65
$[B_{12}H_{12}]^- + e^- \rightarrow [B_{12}H_{12}]^{2-}$	1.93	1.16	−3.55
$[BH_4]^- + e^- \rightarrow [BH_4]^{2-}$	−4.52	−5.22	−9.62
$[BF_4]^- + e^- \rightarrow [BF_4]^{2-}$	−4.07	−4.78	−9.59
$[B_{12}H_{12}]^{2-} + e^- \rightarrow [B_{12}H_{12}]^{3-}$	−4.42	−5.31	−10.70

a. For comparison, SHE of 4.28 V was assumed for all calculations. Note that the absolute potential of SHE in nonaqueous solution is different from that in water.

Note: The choice of the exchange-correlation functional and the solvation model can both result in discrepancies between the experimental and theoretical values. The calculations presented here are used to draw comparisons related to stability trends of the ions rather than to match the experimental values which may be also depend on interactions with other ions/solvent molecules.[5, 11]

SI Table 2: Calculated SCF energies, SCF energies with thermal free energies and SCF energies with solvent (water and THF) effects.

	SCF energy [hartree]	SCF energy with thermal free energies [hartree]	SCF energy with solvent effects [hartree]	
			water	THF
BH_4	−27.158391	−27.146491	−27.162833	-27.161870
$[BH_4]^-$	−27.275238	−27.259678	−27.380328	-27.367015
$[BH_4]^{2-}$	−27.073454	−27.063419	−27.365855	-27.327050
BF_4	−424.420693	−424.436717	−424.430585	-424.427223
$[BF_4]^-$	−424.679695	−424.691373	−424.781676	-424.768528
$[BF_4]^{2-}$	−424.480287	−424.496328	−424.785161	-424.745620
$[B_{12}H_{12}]^-$	−305.729834	−305.602072	−305.790342	-305.564486
$[B_{12}H_{12}]^{2-}$	−305.762852	−305.628769	−306.024792	-305.782893
$[B_{12}H_{12}]^{3-}$	−305.538033	−305.392814	−306.030757	-305.989224

SI Table 3: Calculated $\Delta G_{E.A.}$, $\Delta\Delta G_{solv}$, ΔG_{sol} and $E°_{abs}$ values.

	$\Delta G_{E.A.}$ [kcal/mol]	$\Delta\Delta G_{solv}$ [kcal/mol][a]		ΔG_{sol} [kcal/mol]		$E°_{abs}$ [V]		
		water	THF	water	THF	Water	THF	Gas phase
$BH_4 + e^- \rightarrow [BH_4]^-$	−71.03	−63.16	−55.41	−134.18	−126.43	5.82	5.48	3.08
$BF_4 + e^- \rightarrow [BF_4]^-$	−159.80	−57.79	−51.65	−217.59	−211.45	9.44	9.17	6.93
$[B_{12}H_{12}]^- + e^- \rightarrow [B_{12}H_{12}]^{2-}$	−16.75	−126.40	−108.76	−143.15	−125.51	6.21	5.44	0.73
$[BH_4]^- + e^- \rightarrow [BH_4]^{2-}$	123.15	−117.54	−101.54	5.61	21.61	−0.24	−0.94	−5.34
$[BF_4]^- + e^- \rightarrow [BF_4]^{2-}$	122.39	−127.32	−110.76	−4.92	11.64	−0.21	−0.50	−5.31
$[B_{12}H_{12}]^{2-} + e^- \rightarrow [B_{12}H_{12}]^{3-}$	148.06	−144.82	−124.27	3.24	23.79	−0.14	−1.03	−6.42

a. $\Delta\Delta G_{solv}$ values were set to zero in the calculations (therefore, $\Delta G_{E.A.} = \Delta G_{sol}$) for the reactions in gas phase.

Synthetic Protocols:

*Synthesis of **1**[*]:* To a mixture of 2.26 g (18.5 mmol) decaborane and 1.00 g (18.5 mmol) magnesium borohydride was added 35 ml diglyme. Hydrogen evolution began immediately upon solvent addition. When hydrogen evolution slowed the mixture was heated to reflux and additional hydrogen evolution began. After refluxing for an additional 2.5 h hydrogen evolution had ceased. Reaction was then cooled to room temperature and solvent removed under vacuum to give a light yellow solid. ^{11}B NMR (128.19 MHz, DMF): ∂ -14.9 ($MgB_{12}H_{12}$, d, ^2J(B-H)=129.0 Hz), -17.2 ($MgB_{11}H_{11}$, d, ^2J(B-H)=132.6 Hz), -19.9 ($Mg(B_{11}H_{14})_2$, d(br)); IR (ATR): ν_{BH} 2437.

[*]The procedure yields a mixture of boron clusters believed to predominantly consist of $MgB_{12}H_{12}$, $MgB_{11}H_{11}$, and $Mg(B_{11}H_{14})_2$ which are identified by comparison with NMR and IR spectra available in the literature.[12]

*Synthesis of **2**:* Isopropyl magnesium chloride solution (1.65 ml, 3.3 mmol, 2.0 M solution in diethylether) was added to a Schlenk flask containing 0.50 g *m*-carborane (3.4 mmol) dissolved in 10 ml tetrahydrofuran. The resulting solution was then refluxed with stirring for 72 hours before cooling to room temperature. Solvent was removed in-vacuo, and resulting white solid rinsed with diethyl ether (3 X 15 ml). Solid was further dried in-vacuo before being dissolved in THF and filtered to remove a small amount of insoluble material. Filtrate was then dried in-vacuo to give 0.412 g (2.0 mmol assuming formula: $B_{10}C_2ClH_{11}Mg$, 58.8 % yield) of a white solid. Crystals suitable for x-ray diffraction were obtained by layering of pentane onto a concentrated THF solution of **2**. Crystals of this type were also used to obtain the following characterization data[*]: ^{1}H{^{11}B} NMR (399.54 MHz, [D_8]THF): ∂ 3.05 (s, 1H; C–*H*), 2.1 (m (br), 10H; B–*H*); ^{11}B NMR (128.19 MHz, [D_8]THF): ∂ -4.33 (d, ^2J(B-H)=143.83 Hz), -6.93 (d, ^2J(B-H)=125.85 Hz), -8.21 (d, ^2J(B-H)=143.83 Hz), -10.37 (d, ^2J(B-H)=155.81 Hz), -10.93 (d, ^2J(B-H)=151.19 Hz), -13.35 (d, ^2J(B-H)=160.35 Hz), -14.58 (d, ^2J(B-H)=162.64 Hz), -16.85 (d, ^2J(B-H)=183.26 Hz); IR (ATR): ν_{BH} 2557; Elemental analysis calculated for $B_{20}C_4Cl_4H_{22}Mg_3$: C 9.59, H 4.42, N 0, Al 0 Found: C 9.39, H 4.2, N 0, Al < 200 ppm.

[*]As mentioned in the main text, organomagnesium compounds are known to participate in complex solution chemistry. Crystalline material obtained in this manner displays reversible magnesium deposition and stripping when dissolved in THF, and NMR/IR experiments identified only minor differences between the crystalline and bulk samples (see SI Figure 3, 5).

NMR Spectra:

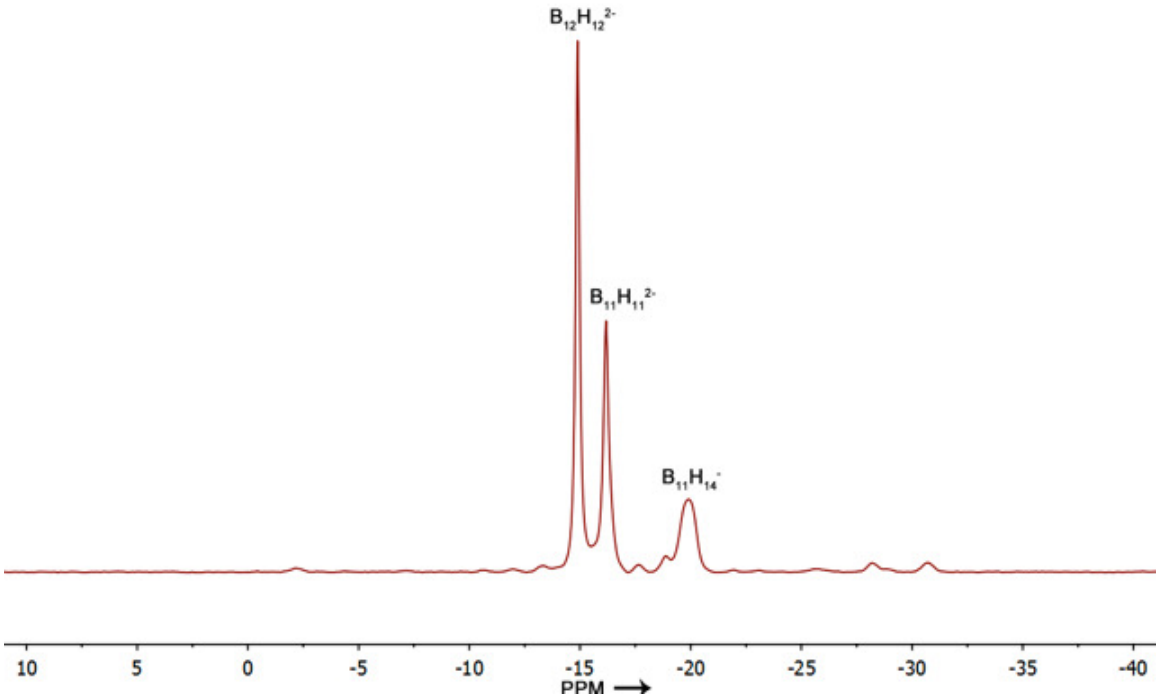

SI Figure 1: $^{11}B\{^{1}H\}$ NMR spectrum of mixture **1**, DMF**.**

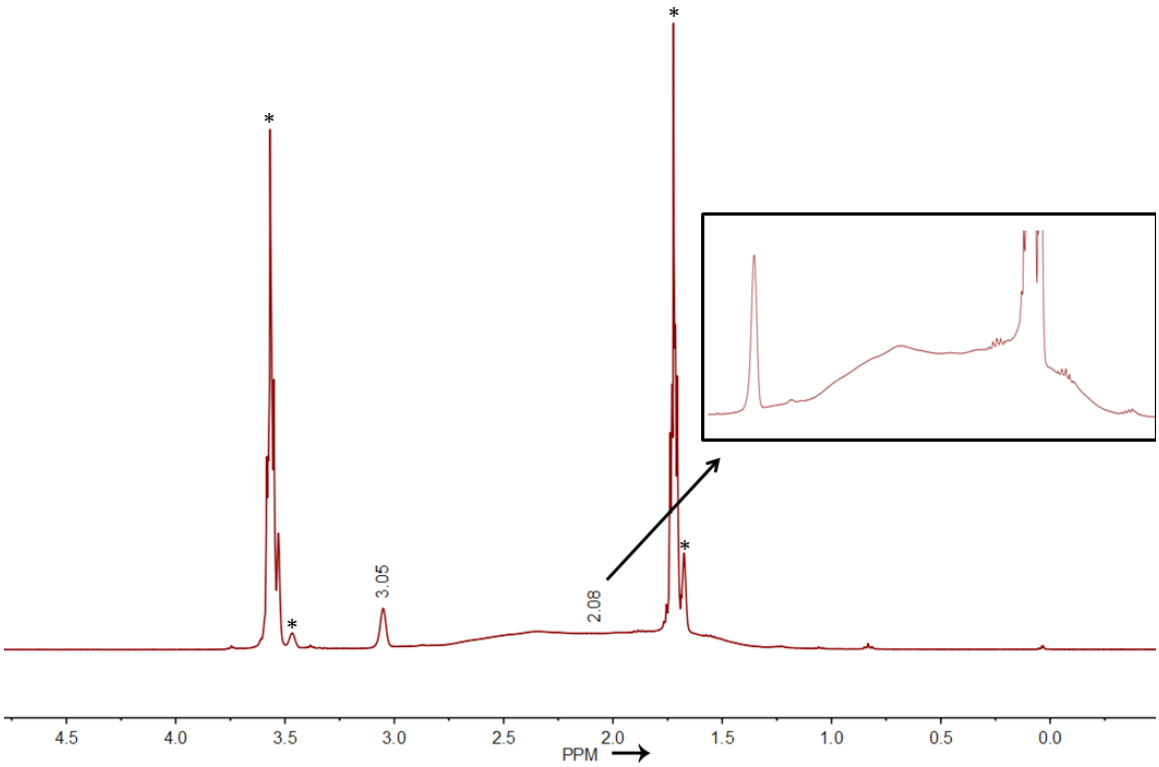

SI Figure 2: $^{1}H\{^{11}B\}$ NMR spectrum of **2**, 399.54 MHz, $[D_8]$THF. * Several THF solvent resonances are observed due protic THF associated with Mg^{2+} cation exchanging with incompletely deuterated $[D_8]$THF.

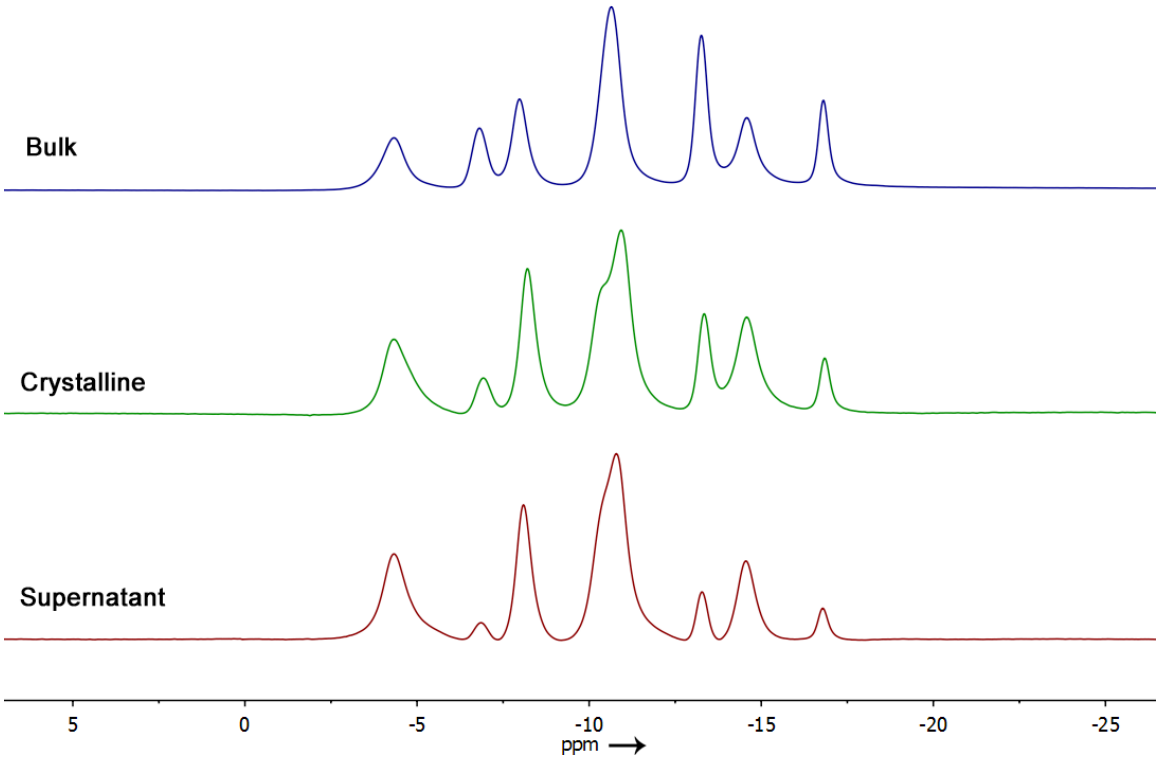

SI Figure 3: Overlay of $^{11}B\{1H\}$ spectra of bulk and crystalline **2** and the supernatant from which the crystals were isolated.

IR Spectra:

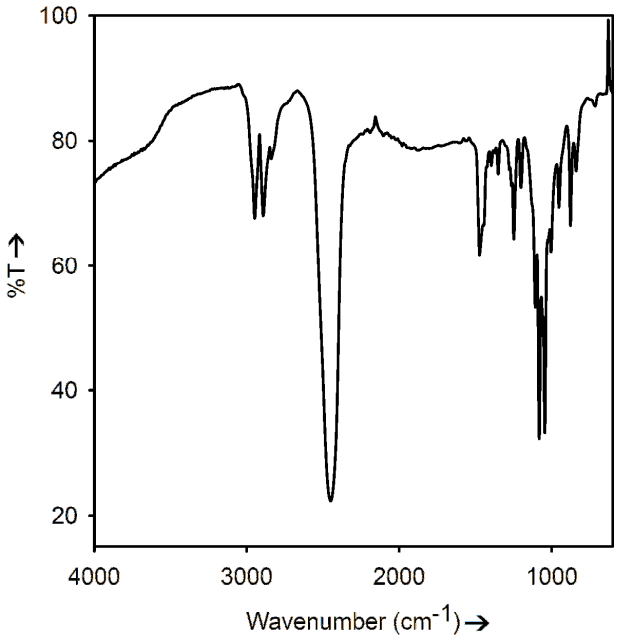

SI Figure 4: FT-IR spectrum of mixture **1**.

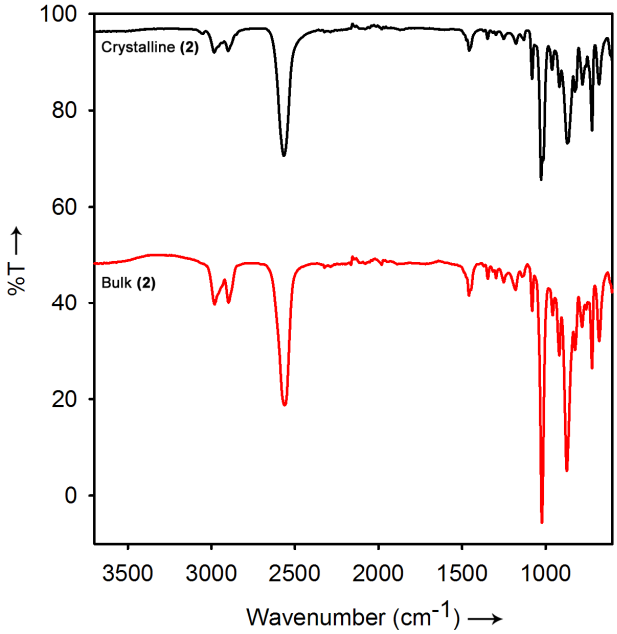

SI Figure 5: Overlay of FT-IR spectra for crystalline and bulk **2**.

Electrochemistry:

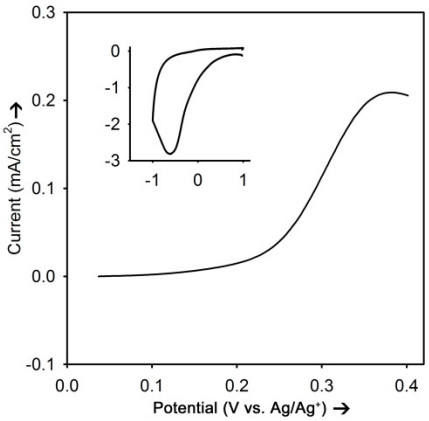

SI Figure 6: Linear scan voltammetry ran on a 17 mg ml^{-1} solution of **1** in propylene carbonate. $Ag/AgNO_3$ reference electrode, Pt working electrode (0.02 cm^2), and Pt wire counter electrode. Inset shows the cyclic voltammetry demonstrating the passivation film formation during the negative scan (ran on a Pt working electrode and Mg reference and counter electrodes).

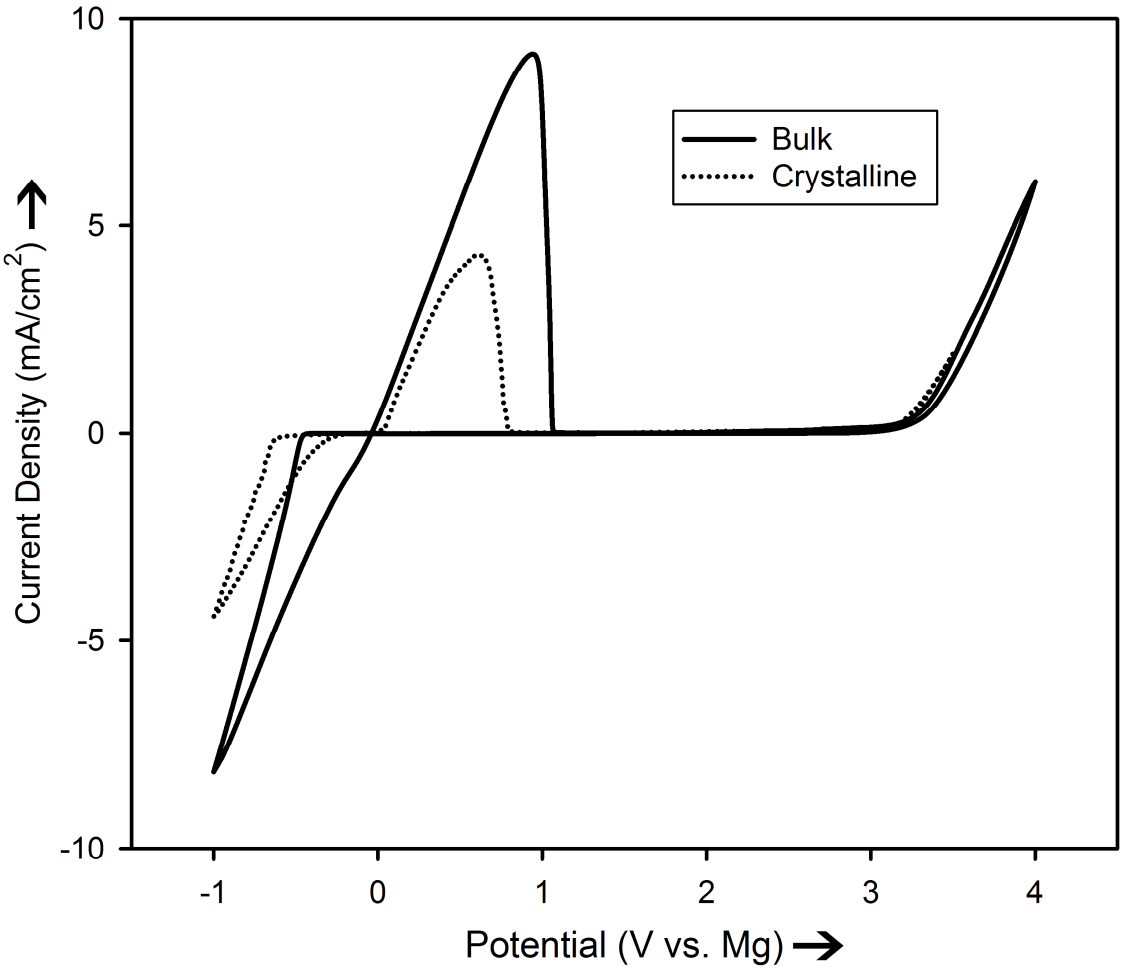

SI Figure 7: Cyclic voltammogram of THF solutions of bulk and crystalline **2** on Pt working electrode (0.02 cm^2). Scan rate 5 mV/s.

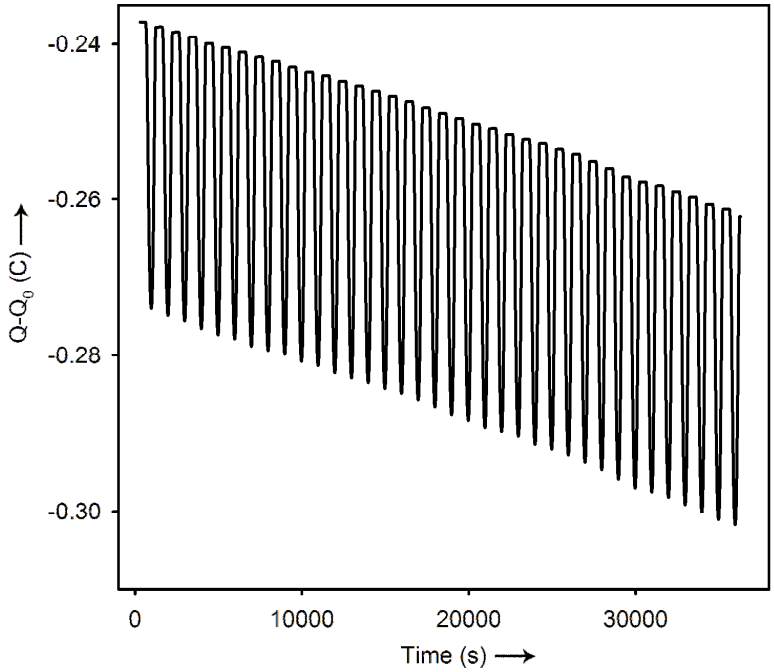

SI Figure 8: Typical Mg deposition and stripping from **2** when cycled (36 times) between -1 and 1.5 V (vs. Mg). Coulombic efficiency > 95 % for all cycles. Pt working electrode (0.02 cm^2). Scan rate: 5 mV/s.

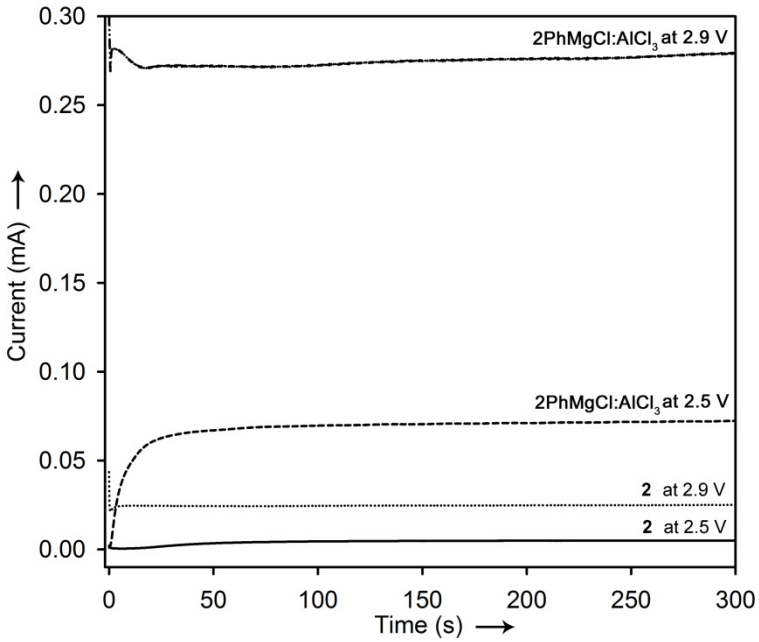

SI Figure 9: Chronoamperometry on solutions of **2** and 2:1 $PhMgCl:AlCl_3$ showing corrosion currents on 316-SS working electrodes at a variety of potentials.

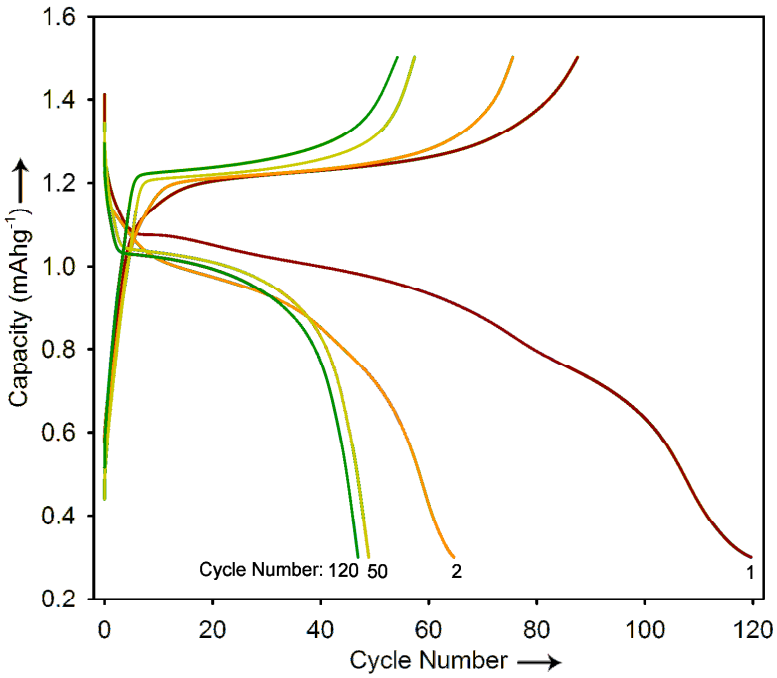

SI Figure 10: Charge/discharge profiles at cycle # 1, 2, 50, and 120 for a rechargeable battery with 2 as the electrolyte run at 100 mA/g, with Mg anode and Chevrel phase cathode. [13]

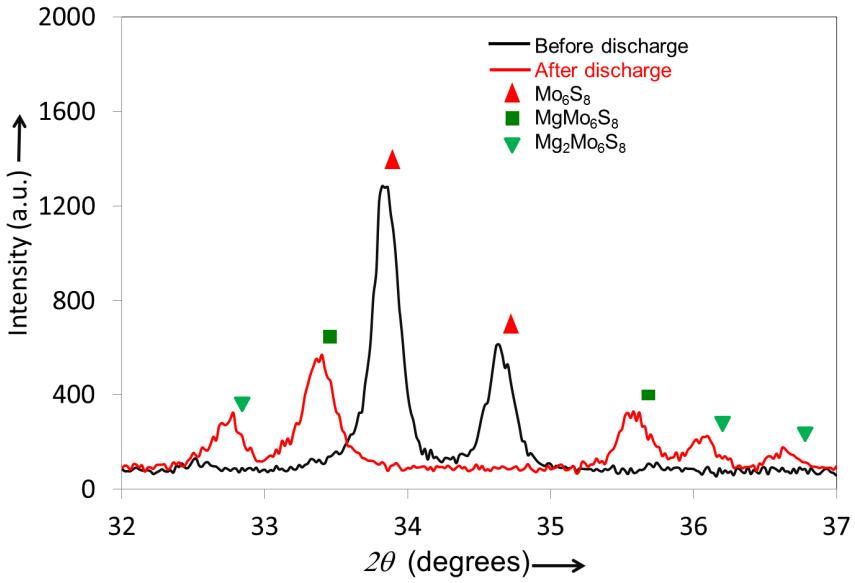

SI Figure 11: XRD results of the cathode before/after discharge illustrating the characteristic peak shifts resulting from the magnesiation of Mo_3S_4.[4c]

X-Ray Crystallographic Data:

Structure Determination of **2**: Colorless plates of **2** were grown from a THF/pentane solution of the compound at ambient temperature. A crystal of dimensions 0.12 x 0.12 x 0.10 mm was mounted on a Rigaku AFC10K Saturn 944+ CCD-based X-ray diffractometer equipped with a low temperature device and Micromax-007HF Cu-target micro-focus rotating anode (l = 1.54187 Å) operated at 1.2 kW power (40 kV, 30 mA). The X-ray intensities were measured at 85(1) K with the detector placed at a distance 42.00 mm from the crystal. A total of 4184 images were collected with an oscillation width of 1.0° in ω. The exposure time was 1 sec. for the low angle images, 4 sec. for high angle. The integration of the data yielded a total of 80912 reflections to a maximum 2θ value of 136.48° of which 9811 were independent and 9143 were greater than 2σ(I). The final cell constants were based on the xyz centroids 38137 reflections above 10σ(I). Analysis of the data showed negligible decay during data collection; the data were processed with CrystalClear 2.0[14] and corrected for absorption. The structure was solved and refined with the Bruker SHELXTL (version 2008/4) software package.[15] Refined Formula: $C_{32}H_{78}B_{20}Cl_4Mg_3O_7$, M_r = 1005.87, Triclinic, space group P -1, a = 11.5952(2), b = 14.5838(3), c = 17.4588(12) Å, α = 70.819, β = 79.147, γ = 81.400°, V = 2726.3(2) $Å^3$, Z = 2, ρ_{calcd} = 1.225 Mgm^{-3}, μ = 2.617 mm^{-1}, reflections collected: 80192, independent reflections: 9811 (Rint = 0.0749), Final R indicies [I > 2σ(I)]: R1 = 0.0413, wR2 = 0.1102, R indicies (all data): R1 = 0.0434, wR2 = 0.1123. CIF file available under CCDC 950050.

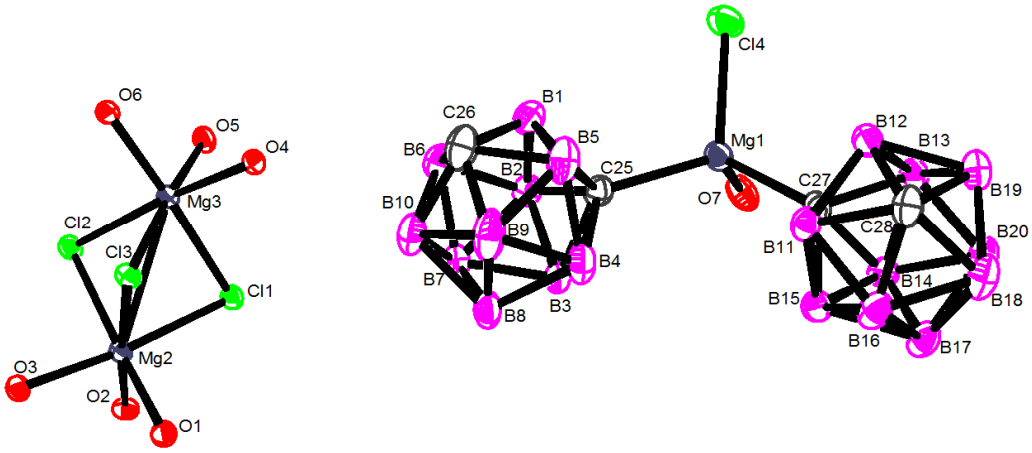

SI Figure 12: Thermal ellipsoid plot of **2** shown at 50% probability. Hydrogen atoms and THF ring carbons (i.e. each oxygen represents a THF solvent molecule) omitted for clarity. Select bond distances (Å) and angles (º): Mg1-O7 2.0336(16), Mg1-C25 2.172(2), Mg1-C27 2.188(2), Mg1-Cl4 2.3119(8), Cl1-Mg2 2.4990(7), Cl1-Mg3 2.5020(7) Mg2-O2 2.0685(14), Mg3-O6 2.0639(14), C25-B5 1.700(3), C25-B1 1.704(3), B1-B5 1.756(4), B2-B6 1.776(3), B4-B5 1.741(4), O7-Mg1-C27 103.75(7), C25-Mg1-Cl4 109.84(6), C27-Mg1-Cl4 113.51(6), Cl3-Mg2-Cl1 85.67(2), O2-Mg2-Cl2 96.81(4), C25-B5-C26 103.33(18).

Supporting References:

[1] R. K. Harris, E. D. Becker, S. M. C. Menezes, R. Goodfellow, P. Granger, *Pure Appl. Chem.* **2001**, *73*, 1795-1818.

[2] a) T. J. Carter, J. W. Kampf, N. K. Szymczak, *Angew. Chem. Int. Ed.* **2012**, *51*, 13168-13172; T. J. Carter, J. W. Kampf, N. K. Szymczak, *Angew. Chem.* **2012**, *52*, 13345-13349; b) M. Daini, M. Suginome, *Chem. Commun.* **2008**, 5224-5226.

[3] R. Mohtadi, M. Matsui, T. S. Arthur, S.-J. Hwang, *Angew. Chem. Int. Ed.* **2012**, *51*, 9780-9783; R. Mohtadi, M. Matsui, T. S. Arthur, S.-J. Hwang, *Angew. Chem.* 2012, *124*, 9918-9921.

[4] a) D. Aurbach, G. S. Suresh, E. Levi, A. Mitelman, O. Mizrahi, O. Chusid, M. Brunelli, *Adv. Mater.* **2007**, *19*, 4260–4267; b) E. Lancry, E. Levi, A. Mitelman, S. Malovany, D. Aurbach, *J. Solid State Chem.* **2006**, *179*, 1879-1882; c) E. Lancry, E. Levi, Y. Gofer, M. Levi, G. Salitra, D. Aurbach, *Chem. Mater.* **2004**, *16*, 2832-2838.

[5] T. B. Lee, M. L. McKee, *Inorg. Chem.* **2012**, *51*, 4205-4214.

[6] M. J. Frisch, G. W. Trucks, H. B. Schlegel, G. E. Scuseria, M. A. Robb, J. R. Cheeseman, G. Scalmani, V. Barone, B. Mennucci, G. A. Petersson, H. Nakatsuji, M. Caricato, X. Li, H. P. Hratchian, A. F. Izmaylov, J. Bloino, G. Zheng, J. L. Sonnenberg, M. Hada, M. Ehara, R. F. K. Toyota, J. Hasegawa, M. Ishida, T. Nakajima, Y. Honda, O. Kitao, H. Nakai, T. Vreven, J. A. Montgomery, J. E. Peralta, F. Ogliaro, M. Bearpark, J. J. Heyd, E. Brothers, K. N. Kudin, V. N. Staroverov, T. Keith, R. Kobayashi, J. Normand, K. Raghavachari, A. Rendell, J. C. Burant, S. S. Iyengar, J. Tomasi, M. Cossi, N. Rega, J. M. Millam, M. Klene, J. E. Knox, J. B. Cross, V. Bakken, C. Adamo, J. Jaramillo, R. Gomperts, R. E. Stratmann, O. Yazyev, A. J. Austin, R. Cammi, C. Pomelli, J. W. Ochterski, R. L. Martin, K. Morokuma, V. G. Zakrzewski, G. A. Voth, P. Salvador, J. J. Dannenberg, S. Dapprich, A. D. Daniels, O. Farkas, J. B. Foresman, J. V. Ortiz, J. Cioslowski, and D. J. Fox, Gaussian 09 Revision C.01 ed., Gaussian Inc., Wallingford, CT, **2010**.

[7] a) C. Lee, W. Yang, R. G. Parr, *Phys. Rev. B* **1988**, *37*, 785-789; b) A. D. Becke, *J. Chem. Phys.* **1993**, *98*, 5648-5652.

[8] R. Krishnan, J. S. Binkley, R. Seeger, J. A. Pople, *J. Chem. Phys.* **1980**, *72*, 650-654.

[9] a) V. Barone, M. Cossi, *Journal Phys. Chem. A* **1998**, *102*, 1995-2001; b) M. Cossi, N. Rega, G. Scalmani, V. Barone, *J. Comput. Chem.* **2003**, *24*, 669-681.

[10] A. A. Isse, A. Gennaro, *J. Phys. Chem. B* **2010**, *114*, 7894-7899.

[11] O. Borodin, W. Behl, T. R. Jow, *J. Phys. Chem. C* **2013**, *117*, 8661-8682.

[12] a) O. Volkov, W. Dirk, U. Englert, P. Paetzold, *Z. Anorg. Allgem. Chem.* **1999**, *625*, 1193-1200; b) E. L. Muetterties, J. H. Balthis, Y. T. Chia, W. H. Knoth, H. C. Miller, *Inorg. Chem.* **1964**, *3*, 444-451; c) H. C. Miller, N. E. Miller, E. L. Muetterties, *Inorg. Chem.* **1964**, *3*, 1456-1463; d) R. L. Middaugh, R. J. Wiersema, *Inorg. Chem.* **1971**, *10*, 423-424; e) V. D. Aftandilian, H. C. Miller, G. W. Parshall, E. L. Muetterties, *Inorg. Chem.* **1962**, *1*, 734-737.

[13] The stable cyclic capacity of 45 mAh g^{-1} is consistent with capacity expected from Chevrel phase Mo_3S_4 ran at these rates and was already contributed to the intrinsic kinetic limitations of this cathode as shown and explained in detail elsewhere: a) H. D. Yoo, I. Shterenberg, Y. Gofer, G. Gershinsky, N. Pour, D. Aurbach, Energy Environ. Sci. 2013, Advance Article, DOI: 10.1039/C3EE40871J; b) D. Aurbach, G. S. Suresh, E. Levi, A. Mitelman, O. Mizrahi, O. Chusid, M. Brunelli, *Adv. Mater.* **2007**, *19*, 4260–4267.

[14] CrystalClear Expert 2.0 r12, Rigaku Americas and Rigaku Corporation (2011), Rigaku Americas, 9009, TX, USA 77381-5209, Rigaku Tokyo, 196-8666, Japan.

[15] Sheldrick, G.M. SHELXTL, v. 2008/4; Bruker Analytical X-ray, Madison, WI, 2008.